

“This document is the Accepted Manuscript version of a Published Work that appeared in final form in *J Am Chem Soc* **2015**, *137* (17), 5845, copyright © American Chemical Society after peer review and technical editing by the publisher. To access the final edited and published work see 10.1021/jacs.5b01526.

HYDROPHOBIC EFFECT AS A DRIVING FORCE FOR HOST-GUEST CHEMISTRY OF A MULTI-RECEPTOR KEPLERATE TYPE-CAPSULE

Nancy Watfa,^{†,‡} Dolores Melgar,^{§,¶} Mohamed Haouas,[†] Francis Taulelle,[†] Akram Hijazi,[‡] Daoud Naoufal,[‡] Josep Bonet Avalos[¶], Sébastien Floquet,[†] Carles Bo,^{*,§,|} and Emmanuel Cadot^{*,†}

[†]Institut Lavoisier de Versailles UMR 8180, Université de Versailles Saint-Quentin, 78035 Versailles, France.

[‡] Université Libanaise, Laboratoire de Chimie de Coordination Inorganique et Organométallique, Campus Universitaire R. Hariri, Faculté des Sciences, Beyrouth, Hadath, Lebanon

[§] Institute of Chemical Research of Catalonia, ICIQ, Tarragona, Av. dels Països Catalans, 16, 43007, Spain.

[¶] Departament d'Enginyeria Química, ETSEQ, Universitat Rovira i Virgili, Av. dels Països Catalans, 26, 43007 Tarragona, Spain

[|] Departament de Química Física i Inorgànica, Universitat Rovira i Virgili, Av. dels Països Catalans, 26, 43007 Tarragona, Spain

ABSTRACT: The effectiveness of the interactions between various alkyl ammonium cations and the well-defined spherical Keplerate-type $\{Mo_{132}\}$ capsule has been tracked by 1H DOSY NMR methodology which reveals a strong dependence of the self-diffusion coefficient of the cationic guests balancing from the solvated to the plugging situations. Analysis of the data is fully consistent with a two-site exchange regime involving the 20 independent $\{Mo_9O_9\}$ receptors of the capsule. Furthermore, quantitative analysis allowed determining the stability constants associated to the plugging process of the pores. Surprisingly, the affinity of the capsule for a series of cationic guests increases continuously with its apolar character as shown by the significant change of the stability constant from 370 to 6500 from NH_4^+ and NEt_4^+ , respectively. Such observations, supported by the thermodynamic parameters evidence that the major factor dictating selectivity in the trapping process is mainly the so-called “hydrophobic effect”. Computational studies, using molecular dynamics simulations have been carried out in the conjunction of the experimental data. The analysis of the radial distribution functions $g(r)$ reveals that NH_4^+ and NMe_4^+ ions behave differently in the vicinity of the capsule. The NH_4^+ ions do not exhibit well-defined distributions in its close vicinity. In contrast, the NMe_4^+ ions were identified as sharp distributions related to different scenario such as firmly trapped or as labile guest facing the $\{Mo_9O_9\}$ pores. These conjugated experimental and theoretical insights should aid the exploitation of these giant polyoxometalates in solution for various applications.

INTRODUCTION

Polyoxometalates (POMs) represent an unprecedented range of discrete anionic metal-oxide clusters which reaches nanoscale in size.¹ Such a class of compounds provides huge potentialities as multifunctional materials with exciting physical and chemical properties for a large set of applications covering biology,² electronics,³ magnetism⁴ and catalysis.⁵ Among the largest existing polyoxometalates, the Keplerate-type polyoxometalates correspond to one of the most fascinating and beautiful arrangement.^{6,7} Resulting from a self-assembling process, the $\{M_{132}\}$ type-Keplerate structure exhibits a high symmetry spheroidal topology combining twelve archetypical pentagonal motifs $\{M(M)_5O_{21}\}$ with $M = Mo$ or W , held together through thirty $\{Mo_2E_2O_2\}$ linkers with $E = O$ or S (see Figure 1).⁸ In addition to the tunable composition of the inorganic skeleton, the nature of the thirty inner ligands can be changed from acetate (for the most classical inner ligand) to specific ligands, thus giving the possibility to tune the inner functionalities of the capsule, such as hydrophobicity/hydrophilicity⁹ and ionic charge.^{10,11}

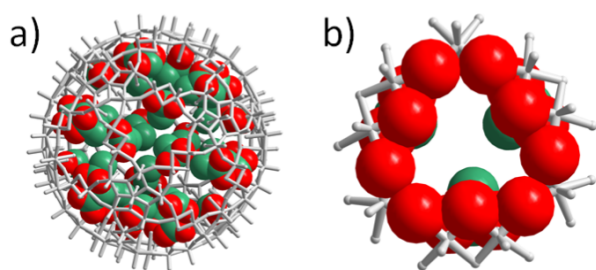


Figure 1. a) Mixed representation (wire and space-filling) of the Keplerate-type anion $\{\text{Mo}_{132}\}$ highlighting the 30 inner acetate ligands (green and red spheres) attached to the inorganic framework (grey stick); b) Highlighting one $\{\text{Mo}_9\text{O}_9\}$ ring/pore.

Nevertheless, the capsule possesses 20 pores lined by $\{\text{Mo}_9\text{O}_6\text{E}_3\}$ rings with C_{3v} local symmetry which have the appropriate size to bind positively charged substrates present in solution. One such remarkable example has been reported with guanidinium cation which fits perfectly the 20 $\{\text{Mo}_9\text{O}_9\}$ pores of the capsule thus revealing an unprecedented polytopic multi-receptor behavior.¹² The Keplerate-type ions gained significant interests as guest trapping or cation carriers, nanosponge or nanoreactor for various applications in materials sciences since specific properties can be engineered chemically simultaneously either in the interior or at the surface of the capsule.¹³ Beside, Keplerate-type ions are able to form very large hollow aggregates which retain the so-called blackberry structure.¹⁴ The complex formation of these “blackberries” aggregates appears mainly governed by the charge density on the surface which can be finely tuned through the control of the ion-pairing process.¹⁵ Then, the full understanding of the plugging process of the 20 pores of the capsule remains an important challenge for further developments in supramolecular chemistry such as i) catalysis in confined environment¹⁶ or at the surface of the capsule,¹⁷ ii) ionic/molecular recognition for ion trapping, iii) the control of the spontaneous self-assembly of “blackberry” aggregates and iv) the design of Keplerate-based materials.¹⁸ In a previous work, we reported that ^1H DOSY NMR methodology can be applied successfully to probe the interactions of the NMe_4^+ cations with the $\{\text{Mo}_9\text{O}_6\text{S}_3\}$ pores of a sulphurated Keplerate, allowing the first quantitative analysis of this type of plugging process.¹⁹ In this paper, we aim to extend this preliminary study to a series of small ammonium cations such as $\text{Me}_{4-x}\text{NH}_x^+$ with $x = 0-4$ in the presence of the large oxo Keplerate $\{\text{Mo}_{132}\}$ ion used as NH_4^+ , Na^+ or Li^+ salts. The ^1H DOSY NMR was used to measure the self-diffusion coefficient D of the NMR probe *i.e.* the tetraalkylammonium ion (TAA) in the presence of the large Keplerate ion $\{\text{Mo}_{132}\}$. These experiments have been carried out at a fixed ratio $\text{TAA}/\{\text{Mo}_{132}\} = 3$ varying the concentration C° in $\{\text{Mo}_{132}\}$ from 0 to 5.10^{-3} mol.L⁻¹. Large changes in D values with concentrations were evidenced and correlated to the plugging process of the TAA at the surface of the $\{\text{Mo}_{132}\}$ ion. Furthermore, the analysis of the D variations versus concentration allows identifying a competitive process at the binding sites between TAA cations and the other counter ions present in solution *i.e.* NH_4^+ , Na^+ or Li^+ . These results reveal that the binding constant correlates nicely with the apolar character of the TAA cation, which could be interpreted as a process mainly governed by the desolvation of the TAA ion balancing between entropic and enthalpic opposite contribution. In addition, the series of studied substrates has been extended to the guanidinium and N,N' Methyl-Ethyl imidazolium cations. We also propose high-level molecular dynamics simulations which shed light on the nature of the interactions between the cation and the large Keplerate ion. Furthermore, computational studies evidenced markedly the distinct behavior between the apolar NMe_4^+ and the ammonium NH_4^+ cation in the vicinity of the $\{\text{Mo}_{132}\}$ surface.

RESULTS AND DISCUSSION

^1H NMR DOSY Analysis. The ammonium salt of the Keplerate $(\text{NH}_4)_{52}[\text{Mo}_{132}\text{O}_{372}(\text{CH}_3\text{COO})_{30}(\text{H}_2\text{O})_{72}].300\text{H}_2\text{O}. 10 \text{ CH}_3\text{COO}$, abbreviated $(\text{NH}_4)_{52}\{\text{Mo}_{132}\}$ has been used as precursor^a for preparation of the sodium and lithium salts $\text{Y}_{52}\{\text{Mo}_{132}\}$ with $\text{Y} = \text{Na}$ or Li . The ^1H NMR spectra of the $\text{NMe}_4\text{Cl}-\text{Y}_{52}\{\text{Mo}_{132}\}$ mixture in aqueous solution show similar features in the range of used concentrations and reveal a broad resonance at 0.5 ppm attributed to the internal acetate coordinated to the $\{\text{Mo}_2\text{O}_4\}$ bridging units, a signal at 1.9 ppm assigned to solvated acetate ions and a narrow signal slightly dependent upon the concentration and ranging from about 3.0 to 3.4 ppm assigned to NMe_4^+ (see supporting information for further NMR details). It could be noted that the linewidth of the NMe_4^+ signal remains almost constant for all the experiments ($\Delta\nu_{1/2} = 1-2$ Hz) meaning that the transverse relaxation time T_2 is almost similar over the concentration range. As usually observed, encapsulated acetate ligands in the Keplerate capsule exhibit the lowest self-diffusion coefficient $D = 115 \pm 5 \mu\text{m}^2.\text{s}^{-1}$ while solvated acetate ions lead to $D = 730 \pm 30 \mu\text{m}^2.\text{s}^{-1}$. The D values for coordinated and solvated acetate species are almost non dependent upon the concentration while the self-diffusion coefficient of the NMe_4^+ ion (D_{obs}) appears strongly affected and varies typically from $D = 910 \pm 50$ to about $190 \pm 20 \mu\text{m}^2.\text{s}^{-1}$. The variation of the self-diffusion coefficient of the encapsulated acetate and that of the NMe_4^+ ion with concentration C° are graphically shown in Figure 2. The dependence of the diffusion coefficient of the NMe_4^+ ion has been interpreted previously as the complexation of the NMe_4^+ ion by the $\{\text{Mo}_9\text{S}_3\text{O}_6\}$ capsule pores and then analyzed as a two-site diffusion system in a fast exchange

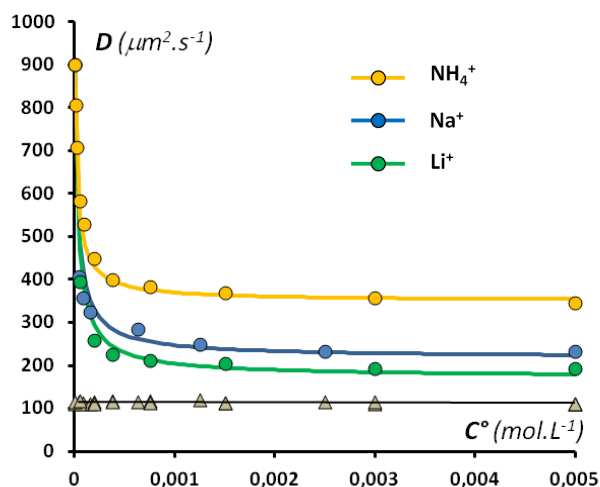
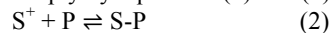


Figure 2. Variation of the self-diffusion coefficient (D) of the NMe_4^+ ions in the presence of different cations (circle) and of the inner acetate ligands (triangle) with concentration in $\{\text{Mo}_{132}\}$ (C°). ^1H DOSY experiments have been carried out at a fixed ratio $\text{NMe}_4^+/\{\text{Mo}_{132}\} = 3$ using three different $\text{Y}_{52}\{\text{Mo}_{132}\}$ salts ($\text{Y} = \text{Li}^+, \text{Na}^+$ or NH_4^+). Experimental data (circles) fit nicely with those calculated (solid lines) using stability constants given in Table 1.

regime.²⁰ In such conditions, the observed diffusion coefficient is the weighted average of the coefficient D^∞ and D° corresponding to the trapped and fully solvated species with the corresponding weights denoted x and $1-x$, respectively. D coefficients are simply related

$$D_{\text{obs}} = xD^\infty + (1-x)D^\circ \quad (1)$$

Interestingly, the limit value of D_{obs} observed for $C^\circ > 2\text{-}3 \cdot 10^{-3} \text{ mol.L}^{-1}$ depends on the nature of the used salt $\text{Y}_{52}\{\text{Mo}_{132}\}$ (with $\text{Y} = \text{Li}, \text{Na}$ or NH_4) and does not reach the expected lowest self-diffusion coefficient value (D^∞) of the Keplerate ion. Such a result is related to a competitive complexation process involving NMe_4^+ and the counter-ions Y^+ . Then, the complexation process of a given substrate noted S^+ should involve two equilibria in competition, involving the twenty $\{\text{Mo}_9\text{O}_9\}$ pores of the capsules (noted P), the counter-ions Y^+ and the cationic substrate S^+ . Assuming that the twenty pores are almost independent,²¹ the host-guest process can be expressed simply by equations (2) and (3).



Analysis of the experimental data using equations (2) and (3) allows calculations of the experimental data of the stability constant K_S and K_Y related to equations (2) and (3), respectively. The values of the stability constants are reported in Table 1 and the satisfactory fits with the experimental data shown in Figure 2. The detailed analytical treatments for calculated data are given in supporting information (SI, section 4). A similar NMR methodology has been applied to determine the stability constant of the alkyl-ammonium series $\text{Me}_{(4-x)}\text{NH}_x^+$. As previously observed with NMe_4^+ ions, the ^1H NMR resonances related to these guest species appear nearly unchanged in the concentration range, allowing a similar analytical method to extract the stability constant K_S from self-diffusion coefficients D_{obs} . The experimental and calculated variations of the self-diffusion coefficient D with concentration C° for these $\text{Me}_{4-x}\text{NH}_x^+$ species are shown in Figure 3 and the corresponding K_S value listed in the Table 1. Stability constant of other cationic guests was obtained by performing similar ^1H DOSY NMR experiments and calculations (See SI, Figure S4 and Table S1); they are also included in the Table 1.

Table 1. Stability constant of alkali, alkyl-ammonium, guanidinium and imidazolium complexes of the multi-receptor Keplerate ions at 30 °C in D_2O .^a

Ions Y^+	Li^+	Na^+	NH_4^+	GuaH^+
Stability constant K_Y	65	130	370	400
Ion S^+	NMe_4^+	HNMe_3^+	H_2NMe_2^+	H_3NMe^+
Stability constant K_S	1550	900	750	475
Ions S^+	Me_3NEt^+	Me_3NPr^+	NEt_4^+	
Stability constant K_S	1800	1600	6500	
Ions S^+	N,N' MethylEthylimidazolium			
Stability constant K_S	5800			

^a The standard error in stability constant is ca 10% as estimated from the accuracy and the reproducibility of the measurements.

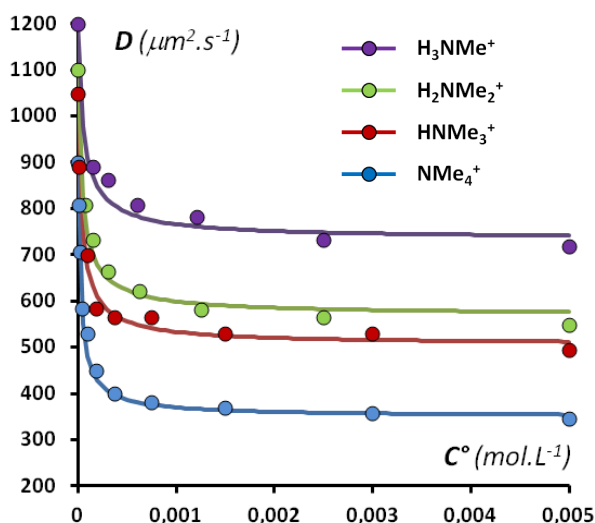


Figure 3. Experimental (circles) and calculated variations (solid lines) of the self-diffusion coefficient of the alkylammonium series $H_{(4-x)}NMe_x^+$ ion (D) with concentration in $\{Mo_{132}\}$ (C°). 1H DOSY experiments have been carried out at a fixed ratio $H_{(4-x)}NMe_x^+/\{Mo_{132}\} = 3$ using $(NH_4)_{52}\{Mo_{132}\}$ salt.

The analysis of the experimental data was performed by assuming that the substrates interact specifically with the 20 pores of the capsules (see SI, section 4). This assumption has been validated by a pore-titration experiment using NMe_4^+ and $Li_{52}\{Mo_{132}\}$ as titrating and titrated reagents, respectively. Such a choice was logically justified by i) the high binding constant of the NMe_4^+ guest (see Table 1), ii) the excellent solubility of the $\{Mo_{132}\}$ capsule in the presence of NMe_4^+ and Li^+ cations allowing to investigate a large range of composition, iii) the lowest stability constant of the lithium cations which is expected to minimize the competition with the NMe_4^+ complexation process. The pore-titration experiment consists of the self-diffusion coefficient measurement of the NMe_4^+ substrate at a fixed concentration in $Li_{52}\{Mo_{132}\}$ ($C^\circ = 1.2 \cdot 10^{-3} \text{ mol.L}^{-1}$) in the presence of variable equivalents of NMe_4^+ ranging from 0 to 50. The basic experimental results (D_{obs} versus $NMe_4^+/\{Mo_{132}\}$) are shown in Figure 4a. The experimental values of D_{obs} allow determining the complexed and solvated NMe_4^+ fractions owing to equation (1), thus giving

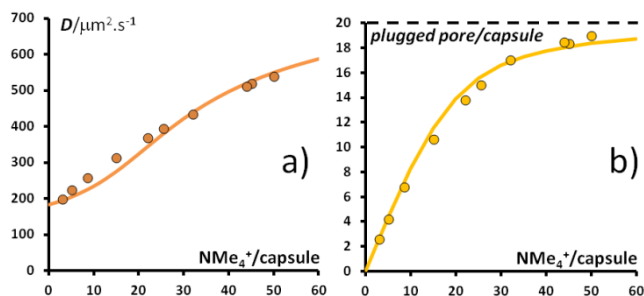
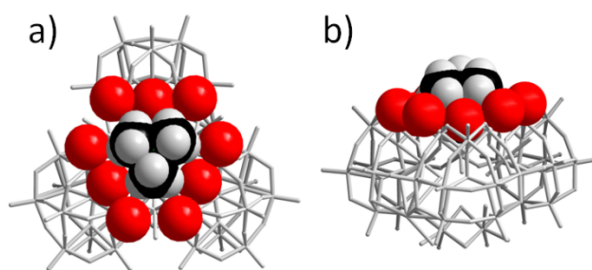


Figure 4. Pores titration experiment $xNMe_4^+ + Li_{52}\{Mo_{132}\}$: a) Variation of the self-diffusion coefficient (D) of the NMe_4^+ with $x = NMe_4^+/\{Mo_{132}\}$; b) Bound NMe_4^+ ions per capsule (plugged pores) versus $x = NMe_4^+/\{Mo_{132}\}$. For both curves, solid lines correspond to calculated data using stability constants $K_s = 1550$ and 65 for NMe_4^+ and Li^+ , respectively (see Table 1).

the number of pores plugged by NMe_4^+ per capsule. As shown in Figure 4b, this number tends consistently toward twenty as the NMe_4^+ concentration increases, fully justifying a twenty pores involvement within equilibria (2) and (3). Furthermore, the calculated data obtained from the stability constants of NMe_4^+ and Li^+ (see Table 1) reveal to be fairly consistent with the experimental ones (see Figure 4), showing that the multi-receptor properties of the capsule can be analyzed simply from a 20 independent-pores model.

The experimental data analysis and their related results given as stability constants lead to many issues for which justifications and interpretations are listed above.

i) The analytical treatment assumes that the cationic guest such as NMe_4^+ ions interacts specifically with the 20 $\{Mo_9O_9\}$ pores. Such a specific interaction can be justified regarding some previous published results. Changing the nature of the pore from $\{Mo_9O_9\}$ to $\{Mo_9S_3O_6\}$ leads to a drastic decrease of the stability constant from $K_s = 1550 \pm 200$ to 210 ± 20 while the main features of the capsule (ionic charge, size and shape) remain almost unchanged.¹⁹ The rationale of such a result is the larger ionic radius of the sulfur atom which reduced the inner space of the pore and then increases the unfavorable steric effect for the NMe_4^+ plugging. We tried to get X-ray diffraction structural data to support these solution studies. The NMe_4^+ salt of $\{Mo_{132}\}$ gave well-shaped crystals but whatever the acquisition conditions, these single-crystals produce only very weak and diffuse diffraction spots, unsuitable for any structural resolution. However, existence of specific interaction can be supported structurally by a host-guest arrangement previously published which involves a NMe_4^+ ion and a single pore-model polyoxometalate (see Figure 5).²² This species consists of three $\{AsW_9O_{33}\}^9-$ subunits



linked together by three $\{O=W-OH_2\}^{4+}$ units. The POM framework

Figure 5. X-ray structure of a single-pore model showing the specific host-guest association between the NMe_4^+ cation and the $\{W_9O_9\}$ pore within a polyoxometalate (data obtained from ref. [22]). a) Top view along the C_3 axis ; b) side view highlighting the $\{W_9O_9\}$ pore filled by one methyl head.

lines a triangular cavity $\{W_9O_9\}$ which exhibits very close structural features that those observed for the $\{Mo_9O_9\}$ pores of the Keplerate ion (depicted in Figure 1b).^{6a} For instance, the perimeter drawn by the nine oxygen atoms is about 25 Å for the $\{Mo_9O_9\}$ pore and ~27 Å for $\{W_9O_9\}$ core. Strikingly, a NMe_4^+ ion has been located within the central hole giving a host-guest arrangement which retains the C_{3v} symmetry with one methyl head plugged within the hole. Surprisingly, the C-H...O distances are long enough (3.4-3.6 Å) to exclude any hydrogen bonds formation as the prime factor of the host-guest stability. Then, the host-guest arrangement involving the $\{Mo_9O_9\}$ pores of the capsule and the Me_4N^+ is probably close to that represented in Figure 5. Last but not least, specific interaction between the NMe_4^+ ion and the 20 pores of the capsule has been nicely demonstrated by a pore-titration experiment (see Figure 4b).

ii) The $\{Mo_9O_9\}$ pores of the Keplerate ion have been previously compared to the [27]-crown-9 macrocycle because both behaves as a guanidinium receptor.¹³ It has been shown that the hexacarboxylate derivative of the [27]-crown-9 macrocycle produces stable complexes in aqueous solution for which the NH_4^+ ion gives the most stable complex while the host-guest stability decreases markedly as the number of methyl group increases in the ammonium $H_{(4-x)}NMe_x^+$ series.²³ Lehn et al. attribute the strong decrease of the stability to steric hindrance between the bulky substituents attached to the macrocycle and the methyl groups of the cation. Surprisingly, the opposite trend is observed specifically using the $\{Mo_{132}\}$ ion. The stability constant increases moderately and continuously from NH_4^+ ($K_s = 370$) to NMe_4^+ ($K_s = 1550$). Such an opposite tendency is nicely shown plotting $\ln K_s$ versus the number of methyl groups noted n_{Me} (see Figure 6). Additionally, the correlation could be even extended with Me_3NEt^+ and Et_4N^+ cationic guests which appear strongly complexed by the $\{Mo_{132}\}$ ion, leading to larger stability constants (1800 and 6500, respectively). As previously mentioned by Lehn *et al.* electrostatic interactions contribute importantly to the stability of the complexes as the main *pull* factor in the inclusion process. But in this present case, the increase of the K_s values as the hydrophobic character of the cation increases highlights the

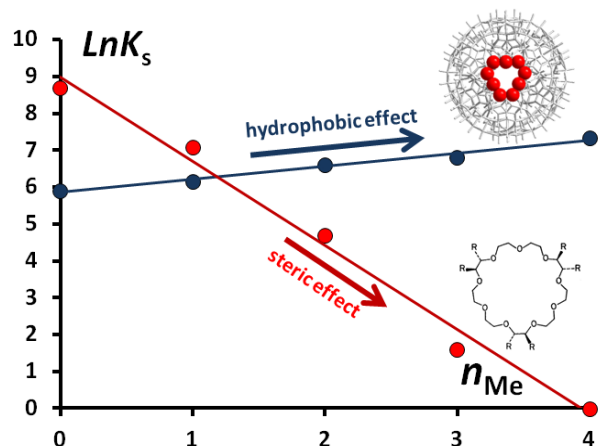


Figure 6. Correlation between $\ln K_s$ and the number of the methyl substituents within the $H_{(4-x)}NMe_x^+$ alkyl-ammonium series obtained with the Keplerate-type ion $\{Mo_{132}\}$ (blue circles) and the hexacarboxylate [27]-crown- O_9 macrocycle (red circles) (data from ref. [23]).

contribution of the polar solvent *i.e.* H_2O , which produces a *push* factor within the complexation process. Such an effect is well documented²⁴ and mainly dictated by the thermodynamic parameters of the ions solvation. Then, cations with weak hydration enthalpies *i.e.* such as apolar cations²⁵ are preferentially trapped within the pores. The complexation processes is spontaneous, however, due to the large entropy gain arising from the release of “structured” water molecules surrounding the hydrophobic hole created by the apolar cation. Furthermore, in the periphery of the $\{Mo_9O_9\}$ pores, there is no attached bulky unit which could be responsible of some unfavorable steric effect. This is precisely the reason why the host-guest stability increases monotonously with the introduction of apolar substituents in the cation. Such a tendency is comparable in some extent to that found by Raymond *et al.* on the encapsulation of apolar ions into supramolecular tetrahedral $[M_4L_6]^{12-}$ anionic hosts.²⁶

Variable temperature ^1H DOSY NMR experiments have been carried out to get more insights into the plugging process with the $\Delta_r H^\circ$ and $\Delta_r S^\circ$ thermodynamic parameters. Such a study was performed using selected $\text{S}-(\text{NH}_4)_{52}\text{Mo}_{132}$ chemical systems such as $\text{S} = \text{NMe}_4^+$ or H_2NMe_2^+ . Experimentally, we monitored that any artifacts, especially convection motions does not interfere on the self-diffusion coefficients measurements in the temperature range restricted to a narrow range between 26 and 42 °C. VT ^1H DOSY NMR details are given in supporting information (SI, section 5). Moreover, the individual binding constants K_s and K_y were calculated from self-diffusion coefficients measured at two different concentrations, such as 3.10^{-4} and 5.10^{-3} mol.L $^{-1}$ and determined for five different temperatures. The thermodynamic parameters $\Delta_r H^\circ$ and $\Delta_r S^\circ$ obtained from the corresponding van't Hoff analysis (see SI, Figure S4) are summarized in Table 2. In general, we found that the plugging of the pores (which exhibit anionic character) by a cationic guest is enthalpically favored ($\Delta_r H^\circ < 0$) and leads to a loss of entropy ($\Delta_r S^\circ < 0$). The decrease of enthalpy is related to dominant electrostatic host-guest interactions while the loss of entropy is rather consistent with the loss of degrees of freedom through the guest assembling into the pore of the large Keplerate ion. However, we found that enthalpy fall in the same range for the studied cations (-29 ± 5 kJ mol $^{-1}$) while entropy shows contrasted differences related to the hydrophobicity of the guest, such as $\Delta_r S^\circ(\text{NH}_4^+) < \Delta_r S^\circ(\text{Me}_2\text{NH}_2^+) < \Delta_r S^\circ(\text{Me}_4\text{N}^+)$ (see Table 2). It seems quite reasonable to assume that a small hydrophilic cation such as NH_4^+ or Li^+ cation remains its solvation sphere intact over the plugging process while bigger hydrophobic cationic guests like NMe_4^+ undergo desolvation causing an entropy gain. Finally, considering equation (4) which expressed the guest exchange process involving the release of a solvated hydrophilic cation Y^+ such as NH_4^+ and the trapping of a hydrophobic S^+ species, the net enthalpy change is close to zero and the entropy change becomes positive meaning that the guest exchange is entropically driven in agreement with the claimed hydrophobic effect.

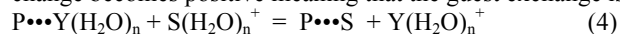


Table 2. Thermodynamic parameters for the plugging process of selected guests.

Ions	NH_4^+	H_2NMe_2^+	NMe_4^+
$\Delta_r H^\circ$ (kJ.mol $^{-1}$) ^a	-34	-24	-23.5
$\Delta_r S^\circ$ (J.mol $^{-1}$ K $^{-1}$) ^a	-64	-31	-17.5

^a The standard error in thermodynamic parameters is ca 20% as estimated from the accuracy and the reproducibility of the measurements

Computational Studies. Complementary insights about interactions between the Keplerate ion with its 42 counter-ions are obtained from molecular dynamics simulations. Calculations have been carried out on the system Keplerate, water and NMe_4^+ or NH_4^+ salts because the latter exhibit contrasted affinity for the Keplerate ion (see Table 1). The $\{\text{Mo}_{132}\}$ anion used in these theoretical investigations contains 30 inner formate ligands inside the capsule, instead of the acetates used in the experimental study. The total charge of the anion is the same in both, experimental and simulated cases and the exact nature of the inner medium of the capsules is expected to play no significant role in the overall dynamics of the capsule and the outer medium. The simulations have been carried out in a box of dimensions $7 \times 7 \times 7$ nm 3 that contains one Mo_{132} anion, the corresponding 42 counter-cations, and 11000 water molecules, leading to a density of 1.06 g.cm $^{-3}$, and to a concentration in Keplerate $C^\circ = 0.0048$ mol.L $^{-1}$. Full computational details, which are equivalent to those used in previous studies,²⁷ are given in the supporting information (SI, section 5). The analysis of the molecular dynamics simulations for NMe_4^+ and NH_4^+ demonstrates clearly that both ions interact differently with the capsule. Two representative snapshots of the dynamics scenario are given in Figure 7, together with the corresponding distribution of cations from the center of the capsule, $g(r)$. According to the $g(r)$ distribution, about 17 NMe_4^+ ions among the 42 are located in the vicinity of the capsule. Few of them corresponding to the closest region ($r < 15$ Å) plug perfectly the pore (see the center of the picture in Figure 7a), even showing exactly the same host-guest arrangement as that observed from the X-Ray structure of the single-pore model mentioned above (Figure 5). A large number of NMe_4^+ cations remain close to the capsule surface for rather long time; some of them located just over the pores and preferentially oriented as the plugging ones (Figure 7a). These correspond to the second peak ($15 < r < 17.7$ Å) shown in Figure 7c and involve about 16 NMe_4^+ ions. The remaining cations observed at $r > 17.7$ Å did not show any specific attraction to the pore structure and simply remain close to the capsule due to its electrostatic inter-

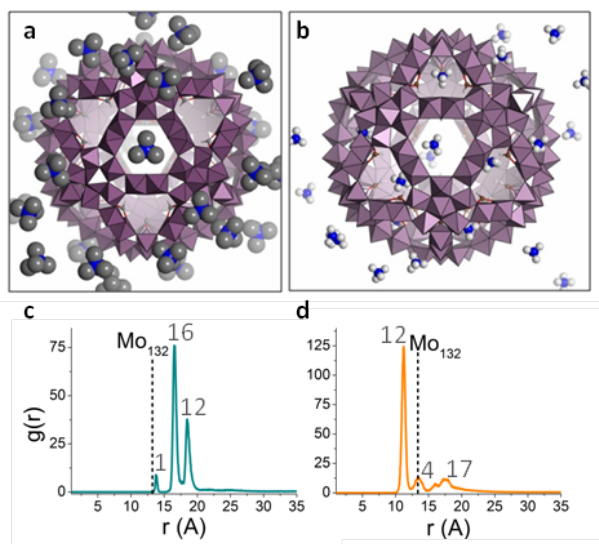


Figure 7. Upper part : snapshots of the MD simulations for NMe_4^+ (a) and NH_4^+ (b) counter-ions in the presence of the $\{\text{Mo}_{132}\}$ ionic capsule; Lower part: radial distribution functions for the (c) NMe_4^+ (blue), (d) NH_4^+ (orange) where the average number of cations associated to each peak has been indicated.

action. Furthermore, none of the NMe_4^+ ions entered into the capsule. In the presence of NH_4^+ , the scenario is quite different. Firstly, some of the ammonium cations enter the capsule, although they remain close to the pores, according to the first peak located at $r = 11,25 \text{ \AA}$ which correspond to the inner space just behind the meta-oxo framework (see Figure 7d). Some of the rest are located just at the pores (second peak in Figure 7d), while the remaining NH_4^+ ions are located close to the capsule surface but not as tightly bound to the latter as NMe_4^+ ions. The presence of clear and well-separated peaks in the distribution functions $g(r)$ computed for both cations (see Figure 7 c-d) corresponds to different dynamic regimes correlated to diffusion coefficients. These different diffusion coefficients collected in Table 3, have been obtained by only considering ion trajectories such that the ion remains inside a given region around the peak for more than 90% of the time window used to determine the mean square displacement (100 ps). Bound cations are expected to diffuse and rotate with the capsule, and its measured diffusion coefficient should scale as r^2 , according to:

$$D_{\text{ion}}(r) = D_{\text{trans}} + D_{\text{rot}}r^2 \quad (4)$$

where D_{trans} is the diffusion coefficient of the center of the $\{\text{Mo}_{132}\}$ capsule, and D_{rot} its rotational diffusion coefficient. The diffusion coefficients of the different components of the system as a function of r^2 are shown graphically in Figure 8. The behavior described in equation (4) should be limited to short simulation times, smaller than $\frac{L}{D_{\text{trans}}}$, estimated to be in the order of 5 ns for our system. The graph in Figure 8 shows clearly that diffusion coefficients associated to the center of the $\{\text{Mo}_{132}\}$, to the Mo atoms, and to the formate hydrogen atoms, as well as those associated to the cations belonging to the first two peaks in $g(r)$ lay in a linear correlation, thus giving a clear indication that these components move together with the capsule. In contrast, free or loosely bound ions should exhibit diffusion coefficients expected to fall well above these correlations. This is exactly observed for ions belonging to the region 3 (see Figure 8). Moreover, it is worth noting that the regression lines depend on the nature of the counterions *i.e.* NH_4^+ or NMe_4^+ . The different behavior is due to the effect of the bound ions on the hydrodynamic drag including strongly bound ions and the surrounding water solvation shell.

Table 3. Regions considered for the MSD treatment and their related self-diffusion coefficient highlighting the different dynamic regimes.

NH_4^+		NMe_4^+	
Region	$D(\mu\text{m}^2.\text{s}^{-1})$	Region	$D(\mu\text{m}^2.\text{s}^{-1})$
1- $r < 12.5 \text{ \AA}$	112.37 ± 0.26	1- $r < 15 \text{ \AA}$	103.40 ± 0.41
2- $r = 12.55 - 15 \text{ \AA}$	149.70 ± 1.3	2- $r = 15 - 17.7 \text{ \AA}$	126.37 ± 0.28
3- $r = 15 - 22.5 \text{ \AA}$	908.30 ± 3.9	3- $r = 17.7 - 20 \text{ \AA}$	296.35 ± 0.81
4- $r > 22.5 \text{ \AA}$	1509.40 ± 1.0	4- $r > 20 \text{ \AA}$	851.6 ± 1.6

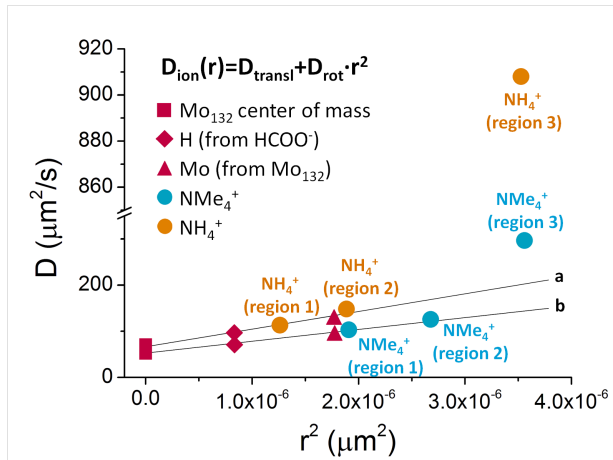


Figure 8. Regression of the self-diffusion coefficient data for different entities of the Mo_{132} capsule (center of mass, H and Mo atoms) (red) for two systems with different counter-cations: NH_4^+ (orange) and NMe_4^+ (blue). The results lay in straight line for each simulation (a for the NH_4^+ system and b for the NMe_4^+ system), which slope is, according to equation (4), the rotational diffusion coefficient ($D_{\text{rot}}(a) = 3.81 \pm 0.24 \cdot 10^7 \text{ s}^{-1}$; $D_{\text{rot}}(b) = 2.56 \pm 0.13 \cdot 10^7 \text{ s}^{-1}$).

Back to Figure 7 c and 7d, we observe that some of the counter-cations are placed indeed very close to the capsule pores, forming a small peak for NMe_4^+ and NH_4^+ at the same distance from the center as the Mo atoms. However, for NMe_4^+ , two high peaks nearby the capsule surface arise from a well-defined distribution of cations. For NH_4^+ , instead, the main peak at 11 \AA corresponds to cations inside the capsule, while the distribution outside the capsule is much less structured than for NMe_4^+ .

The region 1 and 2 where the NH_4^+ ions are located either inside the capsule or in the pore give low D values, close to the experimental one measured for the capsule diffusion (see Table 3). For NMe_4^+ ions, region 1 comprises just one cation directly coordinated to the pore while 16 NMe_4^+ ions in the region 2 remain distributed nearby the capsule surface and located above the pores. Indeed, in this region, the average angle value between the N atoms of NMe_4^+ cations, the center of the capsule and the corresponding pore centroid is

smaller than 10 degrees, indicating that all cations in this region are almost perfectly facing the pores, and that almost all pores are filled. In region 3, which is even further away the surface, NMe_4^+ and NH_4^+ cations behave differently. It is clear from the $g(r)$ profiles and also from the diffusion coefficients that the ammonium cations interact with the capsule weakly than NMe_4^+ . Taking into account that interactions between the capsule and the cations are expected to be stronger with NH_4^+ , because both its high charge density and its ability to form hydrogen bonds,²⁸ the origin of the higher binding constant observed with NMe_4^+ must be related to some “pushing effect”, such as hydrophobic or desolvation effects, previously invoked to explain the variation of the binding constant with the apolar character of the cations. Thus, the molecular dynamics calculations reveal several possible situations for the cations interacting with the large Keplerate ion, thus shedding light for the interpretation of experimental results. The experimental data should be understood as mean values reflecting the distribution of the cations over the different regions surrounding the Keplerate.

CONCLUSION

We have shown that lipophilic cations associate specifically with the $\{\text{Mo}_9\text{O}_9\}$ pores of the Keplerate-type ion which behave like twenty independent effective receptors in aqueous solution. The applied ^1H DOSY NMR methodology able to determine quantitatively the binding constants highlights that apolar cations strongly interact with the $\{\text{Mo}_{132}\}$ Keplerate ion.

These quantitative data, extracted from the self-diffusion coefficients revealed the major factor dictating selectivity in trapping is mainly the so-called “hydrophobic effect”. This suggests that a fine control of the exchange mechanism at the $\{\text{Mo}_9\text{O}_9\}$ pores is achievable which will have broad implications in supramolecular chemistry for i) a regulated access to the large inner cavity, ii) the functionalization of the surface of the capsule, iii) the development of immobilization strategies of Keplerate-type ions on surfaces or within specific matrices. More broadly, as hydrophobic interactions are affected by various factors such as the presence of specific cationic moieties such like ammonium or guanidinium residues, these results demonstrate that control of the hydrophobic strength is possible, opening the way for fine regulations of the interactions between large polyoxometalates and specific hydrophobic patches of biological substrates such as proteins or DNA.²⁹

ASSOCIATED CONTENT

Supporting Information. Materials, instrumentation, preparation of the samples, ^1H NMR (1D, 2D DOSY), vibrational spectroscopy (IR) and analytical analysis for the calculations of the ^1H NMR data, and computational details. This material is available free of charge via the Internet at <http://pubs.acs.org>.

AUTHOR INFORMATION

CORRESPONDING AUTHOR

Emmanuel.cadot@uvsq.fr
cbo@iciq.cat

NOTES

The authors declare no competing financial interests.

ACKNOWLEDGMENT

The authors acknowledge the CNRS (France), the University of Versailles Saint Quentin (France), the ICIQ Foundation, the Spanish Ministerio de Economía y Competitividad (MINECO) through project CTQ2014-52824-R and the Severo Ochoa Excellence Accreditation 2014-2018 (SEV-2013-0319), and the AGAUR of Generalitat de Catalunya through project 2014-SGR-409 for financial support. This project was carried out under the support of the COST Action CM1203 “Polyoxometalate Chemistry for Molecular Nanoscience (PoCheMoN)”. DM gratefully acknowledges URV-ICIQ fellowship.

REFERENCES

-
- (1) (a) Special issue on polyoxometalates: Cronin L. and Müller A. *Chem. Soc. Rev.*, **2012**, *41*, 7333-7334; (b) Dolbecq, A.; Dumas, E.; Mayer, C. R.; Mialane, P. *Chem. Rev.* **2010**, *110*, 6009-6048; (c) Hill, C. L. *Chem. Rev.* **1998**, *98*, 1; (d) Pope, M. T. *Heteropoly and Isopoly Oxometalates*; Springer-Verlag: New York, 1983.
 - (2) Fraqueza, G.; Ohlin, C. A.; Casey, W. H.; Aureliano, M. *J. Bio. Chem.* **2012**, *107*, 82-89.
 - (3) (a) Clemente-Juan, J. M.; Coronado, E.; Gaita-Arino, A. *Chem. Soc. Rev.* **2012**, *41*, 7464-7478; (b) Vilà-Nadal, L.; Mitchell, S. G.; Markov, S.; Busche, C.; Georgiev, V.; Asenov, A.; Cronin L. *Chem. Eur. J.* **2013**, *19*, 16502 – 16511.
 - (4) Baldoví, J. J.; Clemente-Juan, J. M.; Coronado, E.; Duan, Y.; Gaita-Arino, A.; Giménez-Saiz, C. *Inorg. Chem.* **2014**, *53*, 9976-9980.
 - (5) (a) Katryniok, B.; Paul, S.; Capron, M.; Lancelot, C.; Bellière-Baca, V.; Rey, P.; Dumeignil, F. *Green Chem.*, **2010**, *12*, 1922-1925; (b) Katryniok, B.; Paul, S.; Dumeignil, F. *ACS Catal.* **2013**, *3*, 1819 – 1834.
 - (6) (a) Müller, A.; Krickemeyer, E.; Bogge, H.; Schmidtman, M.; Peters, F. *Angew. Chem.-Int. Edit.* **1998**, *37*, 3360; (b) Müller, A.; Peters, F.; Pope, M. T.; Gatteschi, D. *Chem. Rev.* **1998**, *98*, 239-271. (c) Müller, A.; Kögerler, P.; Dress, A. W. M. *Coord. Chem. Rev.* **2001**, *222*, 193-218. (d) Müller, A.; Kögerler, P.; Kuhlmann, C. *Chem. Commun.* **1999**, 1347-1358. (e) Cronin, L.; Beugholt, C.; Krickemeyer, E.; Schmidtman, M.; Bögge, H.; Kögerler, P.; Luong, T. K. K.; Müller, A. *Angew. Chem., Int. Ed.* **2002**, *41*, 2805-2808.
 - (7) Müller, A.; Gouzerh, P. *Chem. Eur. J.* **2014**, *20*, 4862-4873.

- (8) Schäffer, C.; Todea, A. M.; Bögge, H.; Cadot, E.; Gouzerh, P.; Kopilevich, S.; Weinstock, I. A.; Müller, A. *Angew. Chem. Int. Ed.* **2011**, *123*, 12534-12537.
- (9) Schäffer, C.; Todea, A. M.; Bögge, H.; Petina, O. A.; Rehder, D.; Haupt, E. T. K.; Müller, A. *Chem. Eur. J.* **2011**, *17*, 9634-9639.
- (10) Schäffer, C.; Bögge, H.; Merca, A.; Weinstock, I. A.; Rehder, D.; Haupt, E. T. K.; Müller, A. *Angew. Chem. Int. Ed.* **2009**, *48*, 8051-8056.
- (11) (a) Müller, A.; Rehder, D.; Haupt, E. T. K.; Merca, A.; Bögge, H.; Schmidtman, M.; Heinze-Brückner, G. *Angew. Chem. Int. Ed.* **2004**, *43*, 4466-4470; corrigendum: *43*, 5115; (b) Merca, A.; Haupt, E. T. K.; Mitra, T.; Bögge, H.; Rehder, D.; Müller, A. *Chem. Eur. J.* **2007**, *13*, 7650-7658.
- (12) (a) Müller, A.; Krickemeyer, E.; Bögge, H.; Schmidtman, M.; Roy, S.; Berkle, A. *Angew. Chem. Int. Ed.* **2002**, *41*, 3604-3609; (b) Müller, A.; Zhou, Y.; Bögge, H.; Schmidtman, M.; Mitra, T.; Haupt, E. T. K.; Berkle, A. *Angew. Chem. Int. Ed.* **2006**, *45*, 460-465; (c) Müller, A.; Das, S. K.; Talismanov, S.; Roy, S.; Beckmann, E.; Bögge, H.; Schmidtman, M.; Merca, A.; Berkle, A.; Allouche, L.; Zhou, Y.; Zhang, L. *Angew. Chem. Int. Ed.* **2003**, *42*, 5039-5044.
- (13) Müller, A.; Gouzerh, P. *Chem. Soc. Rev.* **2012**, *41*, 7431-7463.
- (14)(a) Liu, T.; Langston, M. L. K.; Li, D.; Pigga, J. M.; Pichon, C.; Todea, A. M.; Müller, A. *Science*, **2011**, *331*, 1590-1592; (b) Mishra, P. P.; Pigga, J.; Liu, T. *J. Am. Chem. Soc.* **2008**, *130*, 1548-1549; (c) Liu, T. *Langmuir*, **2010**, *26*, 9202-9213.
- (15) Kistler, M. L.; Patel, K. G.; Liu, T. *Langmuir*, **2009**, *25*, 7328-7334.
- (16) Kopilevich, S.; Gil, A.; Garcia-Ratés, M.; Bonet-Ávalos, J.; Bo, C.; Müller, A.; Weinstock, I. A. *J. Am. Chem. Soc.*, **2012**, *134*, 13082-13088.
- (17) Rezaeifard, A.; Haddad, R.; Jafarpour, M.; Hakimi, M. *J. Am. Chem. Soc.* **2013**, *135*, 10036-10039.
- (18) Floquet, S.; Terazzi, E.; Korenev, V. S.; Hijazi, A.; Guenee, L.; Cadot, E. *Liquid Crystals*, **2014**, *41*, 1000-1007.
- (19) Korenev, V. S.; Boulay, A. G.; Haouas, M.; Fedin, V. P.; Sokolov, M. N.; Terazzi, E.; Garai, S.; Müller, A.; Taulelle, F.; Marrot, J.; Leclerc, N.; Floquet, S.; Cadot, E. *Chem. Eur. J.* **2014**, *20*, 3097-3105.
- (20) Waldeck, A. R.; Kuchel, P. W.; Lennon, A. J.; Chapman, B. E. *Prog. Nucl. Magn. Reson. Spectrosc.* **1997**, *30*, 39-68.
- (21) Adjacent pores at the surface of the capsule are separated of about 9 Å and then far enough to be considered as nearly independent.
- (22) Pilette, M. A.; Marrot, J.; Duval, S.; Bannani, F.; Floquet, S.; Sécheresse, F.; Cadot, E. *C. R. Chimie*, **2012**, *15*, 124-129.
- (23) Lehn, J.-M.; Vierling, P.; Hayward, R. C. *Chem. Commun.* **1979**, 296-298.
- (24) (a) Aue, D. H.; Webb, H. M.; Bowers, M. T.; *J. Am. Chem. Soc.* **1976**, *98*, 318; (b) Arnett, E. M.; Jones, F. M.; Taagepera, M.; Henderson, W. G.; Beauchamp, J. L.; Holtz, D.; Taft, R. W. *J. Am. Chem. Soc.* **1972**, *94*, 4724; (c) Klots, C. E. *J. Phys. Chem.* **1981**, *85*, 3585.
- (25) (a) Jorgensen, W. L.; Gao, J. *J. Phys. Chem.* **1986**, *90*, 2174-2182; (b) Turner, J. Z.; Soper, A. K.; Finnez, J. L. *J. Chem. Phys.* **1995**, *102*, 5438-5443.
- (26) (a) Parac, T. N.; Caulder, D. L.; Raymond, K. N. *J. Am. Chem. Soc.* **1998**, *120*, 8003-8004; (b) Pluth, M. D.; Tiedemann, B. E. F.; van Halbeek, H.; Nunlist, R.; Raymond, K. N. *Inorg. Chem.* **2008**, *47*, 1411-1413.
- (27) (a) Garcia-Ratés, M.; Miró, P.; Poblet, J.M.; Bo, C.; Bonet Ávalos, J. *J. Phys. Chem. B*, **2011**, *115*, 5980-5992; (b) Garcia-Ratés, M.; Miró, P.; Müller, A.; Bo, C.; Bonet Ávalos, J. *J. Phys. Chem. C*, **2014**, *118*, 5545-5555.
- (28) Interaction energies were computed at a DFT level between the capsule and selected cations. See Table S5 S. I. The computed energies indicate that NH_4^+ interacts stronger with the capsule than NMe_4^+ .
- (29) (a) Ma, C. D.; Wang, C.; Acecco-Vélez, C.; Gellman, S. H.; Abbot, N. L. *Nature*, **2015**, *517*, 347-350; (b) Garde, S. *Nature*, **2015**, *517*, 277-279.

